

Strong and electroweak NLO corrections to Higgs-boson production in vector-boson fusion at the LHC

Mariano Ciccolini^a, Ansgar Denner^a and Stefan Dittmaier^{b*}

^aPaul Scherrer Institut, Würenlingen und Villigen, CH-5232 Villigen PSI, Switzerland

^bMax-Planck-Institut für Physik (Werner-Heisenberg-Institut), D-80805 München, Germany

We present results on the strong and electroweak NLO corrections to the production of a Higgs boson plus two hard jets via weak interactions at the LHC. The calculation includes all weak-boson fusion and quark–antiquark annihilation diagrams as well as all related interferences. We discuss corrections of different origin (QCD corrections of vector-boson-fusion type and interferences, electroweak corrections induced by quark or photonic initial states, heavy-Higgs-boson effects, etc.) and give some new results for distributions for a Higgs-boson mass of 200 GeV. The electroweak corrections are of the same size as the QCD corrections, viz. typically at the level of 5–10% for a Higgs-boson mass up to ~ 700 GeV. In general, they do not simply rescale differential distributions, but induce distortions at the level of 10%. The discussed corrections have been implemented in a flexible Monte Carlo event generator.

1. Introduction

The electroweak (EW) production of a Standard Model Higgs boson in association with two hard jets in the forward and backward regions of the detector—frequently quoted as “vector-boson fusion” (VBF)—is a cornerstone in the Higgs-boson search both in the ATLAS [1] and CMS [2] experiments at the LHC and also plays an important role in the determination of Higgs-boson couplings at this collider.

Higgs+2jets production in pp collisions proceeds through two different channels. The first channel corresponds to a pure EW process. It comprises the scattering of two (anti-)quarks mediated by t - and u -channel W- or Z-boson exchange, with the Higgs boson radiated off the virtual weak boson. It also involves Higgs-boson radiation off a W- or Z-boson produced in s -channel quark–antiquark annihilation (Higgs-strahlung process), with the weak boson decaying hadronically. The second channel proceeds through strong interactions, the Higgs boson being radi-

ated off a heavy-quark loop that couples to any parton of the incoming hadrons via gluons [3].

In the weak-boson-mediated processes, the two scattered quarks are usually visible as two hard forward jets, in contrast to other jet production mechanisms, offering a good background suppression (transverse-momentum and rapidity cuts on jets, jet rapidity gap, central-jet veto, etc.). Applying appropriate event selection criteria (see e.g. Ref. [4] and references in Refs. [5,6]) it is possible to sufficiently suppress background and to enhance the VBF channel over the hadronic Higgs+2jets production mechanism.

In order to match the required precision for theoretical predictions at the LHC, QCD and EW corrections are needed. When VBF cuts are imposed, the cross section can be approximated by the contribution of squared t - and u -channel diagrams only, which reduces the QCD corrections to vertex corrections to the weak-boson–quark coupling. Explicit next-to-leading order (NLO) QCD calculations in this approximation exist since more than a decade [5,7], while corrections to distributions have been calculated in the last few years [8,9]. Recently, the full NLO EW and QCD corrections to this process have be-

*This work is supported in part by the European Community’s Marie-Curie Research Training Network HEP-TOOLS under contract MRTN-CT-2006-035505.

come available [10,11]. This calculation includes, for the first time, the complete set of EW and QCD diagrams, namely the t -, u -, and s -channel contributions, as well as all interferences at NLO. Higher-order loop-induced interference effects between VBF and gluon–gluon fusion have been examined in Refs. [12] and turn out to be completely negligible. Very recently, also the additional supersymmetric QCD and EW corrections within the MSSM have been evaluated [13] and found to be typically below or at the 1% level.

In these proceedings we briefly summarize the calculation of the NLO EW and QCD corrections presented in Refs. [10,11] and give new results on distributions for a Higgs-boson mass of 200 GeV.

2. Brief outline of the NLO calculation

We have calculated the complete QCD and EW NLO corrections to Higgs-boson production via weak VBF at the LHC. At LO, this process receives contributions from the partonic processes $qq \rightarrow Hqq$, $q\bar{q} \rightarrow Hq\bar{q}$, and $\bar{q}\bar{q} \rightarrow H\bar{q}\bar{q}$. All LO and one-loop NLO diagrams are related by crossing symmetry to the corresponding decay amplitude $H \rightarrow q\bar{q}q\bar{q}$. The QCD and EW NLO corrections to these decays were discussed in Ref. [14]. In our calculation of the corrections, which is described in detail in Refs. [10,11], we partially made use of the results on the related Higgs decays. The electroweak NLO corrections have been supplemented by the leading two-loop heavy-Higgs-boson effects [15] proportional to $G_\mu^2 M_H^4$.

In the s -channel diagrams intermediate W and Z bosons can become resonant, corresponding to WH/ZH production with subsequent gauge-boson decay. In order to consistently include these resonances, we use the “complex-mass scheme” at the one-loop level [16], which respects all relations that follow from gauge invariance. In this approach the W- and Z-boson masses are consistently considered as complex quantities, defined as the locations of the propagator poles in the complex plane. The tensor integrals are evaluated using the reduction techniques of Refs. [17,18], which include direct reductions of pentagon integrals to boxes and specific methods to treat exceptional phase-space configurations in

a numerically stable way.

Real corrections consist of gluon and photon emission and processes with gq and γq initial states. The mass singularities from collinear initial-state splittings are absorbed via factorization by the usual PDF redefinition both for the QCD and photonic corrections. Technically, the soft and collinear singularities are isolated in the dipole subtraction method following Refs. [19,20], and the result was checked with the phase-space slicing method.

Each part of the whole calculation has been worked out twice and independently, and all corrections are implemented in a flexible Monte Carlo event generator based on multi-channel integration.

3. Numerical results

Numerical results for the Higgs-mass dependence and the scale dependence of the total cross section with and without VBF cuts as well as distributions for $M_H = 120$ GeV have been presented in Refs. [10,11]. Some distributions for $M_H = 200$ GeV have been published in Ref. [21]. Here we summarize the size of the different contributions to the total cross section and show some more distributions for $M_H = 200$ GeV.

All presented results are based on the input parameters as given in Ref. [11]. Since quark-mixing effects are suppressed, the CKM matrix is set to the unit matrix. The electromagnetic coupling is fixed in the G_μ scheme, i.e. it is set to $\alpha_{G_\mu} = \sqrt{2}G_\mu M_W^2 s_w^2 / \pi$, because this accounts for electromagnetic running effects and some universal corrections of the ρ parameter. We use the MRST2004QED PDF [22] which consistently include $\mathcal{O}(\alpha)$ QED corrections and a photon distribution function for the proton. In our default set-up we use only four quark flavours for the external partons, i.e. we do not take into account the contribution of bottom quarks, which is suppressed. Partonic processes involving b quarks are, however, included in our code in LO. The renormalization and factorization scales are set to M_W , 5 flavours are included in the two-loop running of α_s , and $\alpha_s(M_Z) = 0.1187$. We apply typical VBF cuts to the outgoing jets as described

in detail in Ref. [11].

In Table 1 we summarize the impact of different contributions to the integrated cross sections with and without VBF cuts for Higgs masses between 120 and 200 GeV, for $M_H = 400$ GeV, and for $M_H = 700$ GeV in per cent of the corresponding LO cross section.

Previous calculations of the VBF process [5, 7, 8, 9] have consistently neglected s -channel contributions (“Higgs strahlung”), which involve diagrams where one of the vector bosons can become resonant, as well as the interference between t - and u -channel fusion diagrams. For small Higgs-boson masses the contributions of s -channel diagrams, $\Delta_{s\text{-channel}}$, range between 10% and 30% when no cuts are applied. With VBF cuts, the s -channel contributions are strongly suppressed, yielding less than 0.6% of the cross section for all the studied Higgs-boson masses. The contributions from interferences between t - and u -channel diagrams, $\Delta_{t/u\text{-int}}$, are below 1% with or without VBF cuts and thus negligible. Consequently, applying typical experimental VBF cuts, the contributions from s -channel diagrams and t/u -channel interferences can be safely neglected.

Next, we list in Table 1 the contributions arising at LO from processes that include b -quarks in the initial and/or final states. These are included in our programs but not in the default set-up. For Higgs-boson masses below 200 GeV, they increase the total cross section without cuts by about 4% and the one with cuts by about 2%. For larger Higgs-boson masses their impact is smaller.

In the lower part of Table 1 contributions of various NLO corrections are listed. Both electroweak and QCD corrections are at the level of 5–10%. The QCD corrections are dominated by the previously known diagonal contributions, i.e. by the vector-boson–quark–antiquark vertex corrections to squared LO diagrams, $\delta_{\text{QCD}(\text{diag})}$. All other QCD contributions, i.e. QCD corrections to interferences between the different LO diagrams and interferences with gg -fusion and g -splitting diagrams (see Ref. [11] for a precise definition), summarized in $\delta_{\text{QCD}(\text{int})}$, are at the per-mille level and even partially cancel each other. They are not enhanced by contributions of two t - or u -channel vector bosons with small virtuality and

therefore even further suppressed when applying VBF cuts. For the electroweak corrections we give the impact of the quark–quark induced processes, $\delta_{\text{EW},qq}$, and the one of the photon induced processes, $\delta_{\text{EW},q\gamma}$ separately. The latter turn out to be $\sim +1\%$ and reduce the complete electroweak corrections for small Higgs-boson masses. The dominant two-loop correction $\delta_{G_\mu^2 M_H^4}$ due to Higgs-boson self-interaction, which is contained in $\delta_{\text{EW},qq}$, is completely negligible in the low- M_H region, but becomes important for large Higgs-boson masses and yields +4% for $M_H = 700$ GeV which constitutes about 50% of the total EW corrections. Obviously for Higgs masses in this region and above the perturbative expansion breaks down, and the two-loop factor $\delta_{G_\mu^2 M_H^4}$ might serve as an estimate of the theoretical uncertainty.

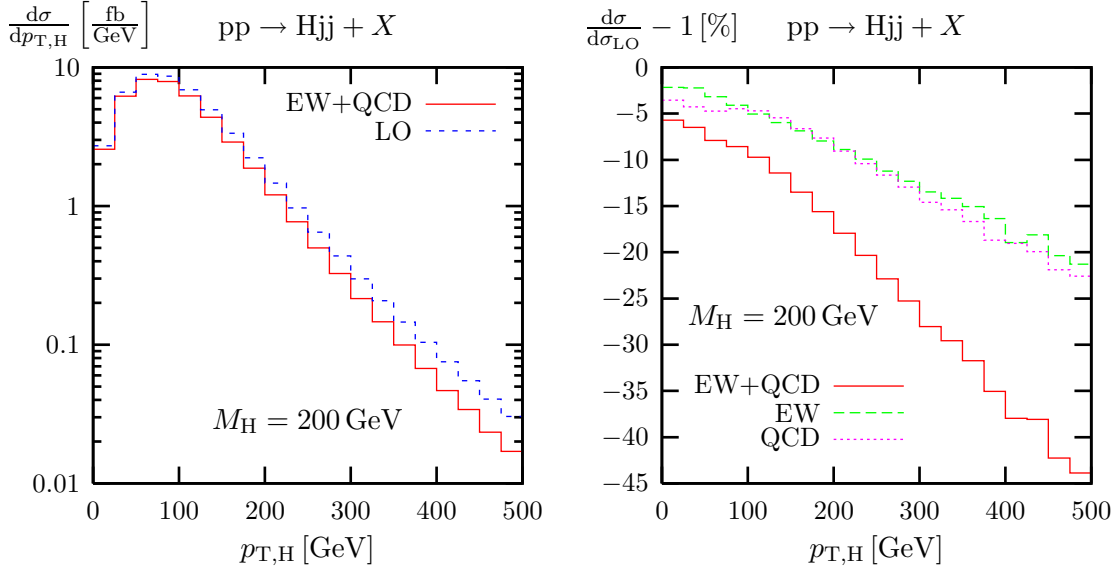
The EW corrections to distributions for $M_H = 200$ GeV are qualitatively similar to those for $M_H = 120$ GeV presented in Ref. [11]. The distributions in the transverse momentum $p_{j1,T}$ of the harder tagging jet j_1 (jet with highest p_T passing all cuts) and the distribution in the azimuthal angle separation of the two tagging jets for $M_H = 200$ GeV have been presented in Ref. [21]. Here we show some additional distributions for $M_H = 200$ GeV.

In Figure 1 we provide the distribution in the transverse momentum $p_{T,H}$ of the Higgs boson. The differential cross section drops strongly with increasing $p_{T,H}$. As for $M_H = 120$ GeV both the relative EW and QCD corrections increase in size and reach -20% for $p_{T,H} = 500$ GeV. Figure 2 shows the rapidity distribution of the Higgs boson. While the QCD corrections distort this shape by about 10%, the relative EW corrections turn out to be flat where the distribution is sizeable. In Figure 3, we depict the distribution in the rapidity of the harder tagging jet. It can be clearly seen that the tagging jets are forward and backward located. The EW corrections vary between -3% and -6% . The QCD corrections exhibit a strong dependence on the jet rapidity. They are about -10% in the central region but become positive for large rapidities, where they tend to compensate the EW corrections. Shape changes due to the full corrections reach 10%.

Table 1

Impact of specific corrections to the cross section without and with VBF cuts relative to LO.

M_H [GeV]	no cuts			VBF cuts		
	120–200	400	700	120–200	400	700
$\Delta_{s\text{-channel}}$ [%]	30–10	2	1	< 0.6	< 0.3	< 0.1
$\Delta_{t/u\text{-int}}$ [%]	< 0.5	< 0.1	< 0.1	< 0.1	< 0.1	< 0.1
$\Delta_{b\text{-quarks}}$ [%]	≈ 4	2	1	≈ 2	2	1
$\delta_{\text{QCD(diag)}}$ [%]	4–0.5	–0	+1	≈ -5	–6	–7
$\delta_{\text{QCD(int)}}$ [%]	$\lesssim 0.2$	–0.2	–0.1	< 0.1	< 0.1	< 0.1
$\delta_{\text{EW,qq}}$ [%]	≈ -5	–5	+6	≈ -7	–5	+5
$\delta_{\text{EW,q}\gamma}$ [%]	$\approx +1$	+2	+2	$\approx +1$	+1	+2
$\delta_{G_\mu^2 M_H^4}$ [%]	< 0.1	+0.4	+4	< 0.1	+0.4	+4

Figure 1. Distribution in the transverse momentum $p_{T,H}$ of the Higgs boson (left) and corresponding relative corrections (right) for $M_H = 200$ GeV.

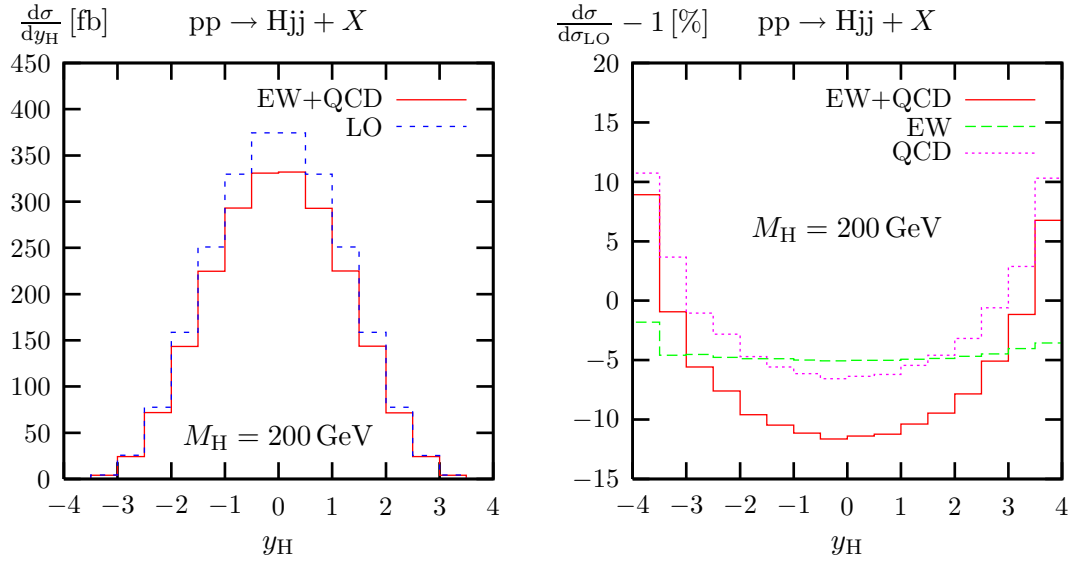


Figure 2. Distribution in the rapidity y_H of the Higgs boson (left) and corresponding relative corrections (right) for $M_H = 200$ GeV.

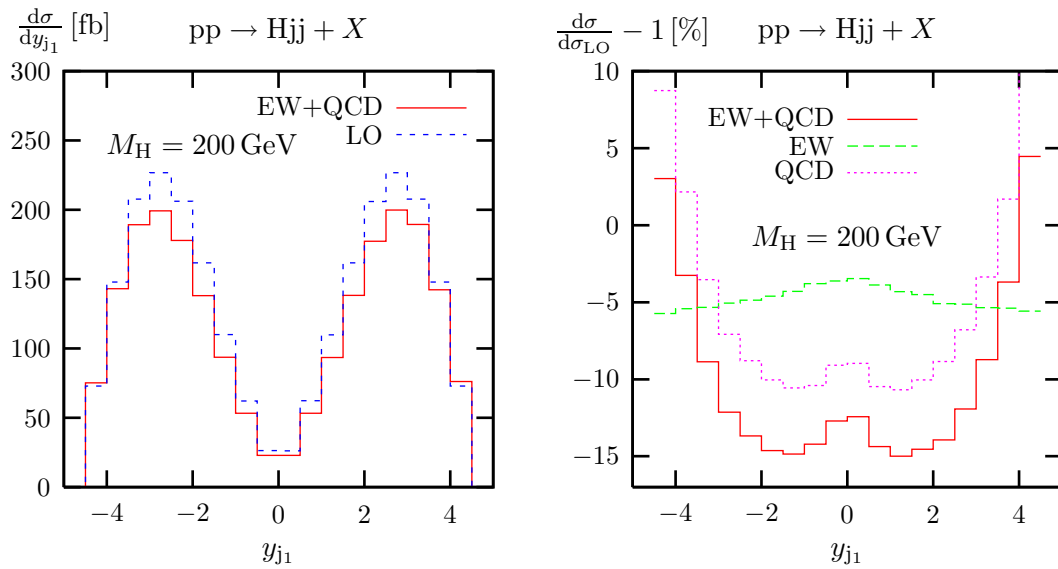


Figure 3. Distribution in the rapidity y_{j_1} of the harder tagging jet (left) and corresponding relative corrections (right) for $M_H = 200$ GeV.

4. Conclusions

Radiative corrections of strong and electroweak interactions have been discussed at next-to-leading order for Higgs-boson production via vector-boson fusion at the LHC. All discussed effects have been implemented into a flexible Monte Carlo generator. The electroweak corrections affect the cross section by 5%, and are thus as important as the QCD corrections in this channel. They do not simply rescale distributions but induce distortions at the level of 10%. Effects from photon-induced processes, s -channel contributions, and interferences are small once vector-boson fusion cuts are applied. For intermediate Higgs-boson masses the remaining theoretical uncertainty is below the uncertainty from PDFs and expected experimental errors.

REFERENCES

1. S. Asai *et al.*, *Eur. Phys. J. C* **32S2** (2004) 19 [hep-ph/0402254].
2. S. Abdullin *et al.*, *Eur. Phys. J. C* **39S2** (2005) 41.
3. V. Del Duca *et al.*, *Nucl. Phys. B* **616** (2001) 367 [hep-ph/0108030];
J. M. Campbell, R. K. Ellis and G. Zanderighi, *JHEP* **0610** (2006) 028 [hep-ph/0608194].
4. V. D. Barger, R. J. N. Phillips and D. Zeppenfeld, *Phys. Lett. B* **346** (1995) 106 [hep-ph/9412276];
D. L. Rainwater and D. Zeppenfeld, *JHEP* **9712** (1997) 005 [hep-ph/9712271];
D. L. Rainwater, D. Zeppenfeld and K. Hagiwara, *Phys. Rev. D* **59** (1999) 014037 [hep-ph/9808468];
D. L. Rainwater and D. Zeppenfeld, *Phys. Rev. D* **60** (1999) 113004 [Erratum-ibid. *D* **61** (2000) 099901] [hep-ph/9906218];
V. Del Duca *et al.*, *JHEP* **0610** (2006) 016 [hep-ph/0608158].
5. M. Spira, *Fortsch. Phys.* **46** (1998) 203 [hep-ph/9705337].
6. A. Djouadi, *Phys. Rept.* **457** (2008) 1 [arXiv:hep-ph/0503172].
7. T. Han, G. Valencia and S. Willenbrock, *Phys. Rev. Lett.* **69** (1992) 3274 [hep-ph/9206246].
8. T. Figy, C. Oleari and D. Zeppenfeld, *Phys. Rev. D* **68** (2003) 073005 [hep-ph/0306109];
E. L. Berger and J. Campbell, *Phys. Rev. D* **70** (2004) 073011 [hep-ph/0403194].
9. T. Figy and D. Zeppenfeld, *Phys. Lett. B* **591** (2004) 297 [hep-ph/0403297].
10. M. Ciccolini, A. Denner and S. Dittmaier, *Phys. Rev. Lett.* **99** (2007) 161803 [arXiv:0707.0381].
11. M. Ciccolini, A. Denner and S. Dittmaier, *Phys. Rev. D* **77** (2008) 013002 [arXiv:0710.4749 [hep-ph]].
12. J. R. Andersen, T. Binoth, G. Heinrich and J. M. Smillie, *JHEP* **0802** (2008) 057 [arXiv:0709.3513 [hep-ph]];
A. Bredenstein, K. Hagiwara and B. Jäger, *Phys. Rev. D* **77** (2008) 073004 [arXiv:0801.4231 [hep-ph]].
13. W. Hollik, T. Plehn, M. Rauch and H. Rzehak, arXiv:0804.2676 [hep-ph].
14. A. Bredenstein, A. Denner, S. Dittmaier and M. M. Weber, *Phys. Rev. D* **74** (2006) 013004 [hep-ph/0604011]; *JHEP* **0702** (2007) 080 [hep-ph/0611234].
15. A. Ghinculov, *Nucl. Phys. B* **455** (1995) 21 [hep-ph/9507240];
A. Frink, B. A. Kniehl, D. Kreimer and K. Riesselmann, *Phys. Rev. D* **54** (1996) 4548 [hep-ph/9606310].
16. A. Denner, S. Dittmaier, M. Roth and L. H. Wieders, *Nucl. Phys. B* **724** (2005) 247 [hep-ph/0505042].
17. A. Denner and S. Dittmaier, *Nucl. Phys. B* **658** (2003) 175 [hep-ph/0212259].
18. A. Denner and S. Dittmaier, *Nucl. Phys. B* **734** (2006) 62 [hep-ph/0509141].
19. S. Dittmaier, *Nucl. Phys. B* **565** (2000) 69 [hep-ph/9904440].
20. S. Dittmaier, A. Kabelschacht and T. Kasprzik, arXiv:0802.1405 [hep-ph].
21. M. Ciccolini, A. Denner and S. Dittmaier, arXiv:0712.2895 [hep-ph].
22. A. D. Martin *et al.*, *Eur. Phys. J. C* **39** (2005) 155 [hep-ph/0411040].